



Article

Fabrication of Enzyme-Free and Rapid Electrochemical Detection of Glucose Sensor Based on ZnO Rod and Ru Doped Carbon Nitride Modified Gold Transducer

Habibulla Imran ^{1,2}, Asrar Alam ¹ , Venkataraman Dharuman ^{2,*} and Sooman Lim ^{1,*}

¹ Department of Flexible and Printable Electronics, LANL-JBNU Engineering Institute, Jeonbuk National University, Jeonju 54896, Korea; imranh091@gmail.com (H.I.); asrarlm0@gmail.com (A.A.)

² Molecular Electronics Laboratory, Department of Bioelectronics and Biosensors, Science Campus, Alagappa University, Karaikudi 630004, India

* Correspondence: dharumanudhay@yahoo.com (V.D.); smlim@jbnu.ac.kr (S.L.)

Abstract: Over 3 in 4 adults with diabetes live in low- and middle-income countries and health expenditure also increased 316% over the last 15 years. In this regard, we fabricate low cost, reusable and rapid detection of diabetes sensor based on zinc oxide rod inserted ruthenium-doped carbon nitride (ZnO-g-Ru-C₃N₄) modified sensor device. Developed sensor device physically and electrochemically characterized using X-ray diffraction (XRD), fourier-transform infrared spectroscopy (FTIR), transmission electron microscopy (TEM), X-ray photoelectron spectroscopy (XPS), cyclic voltammetry (CV), chronoamperometry (CA) and differential pulse voltammetry (DPV). Sensing device as an effective enzyme-free glucose detection with high sensitivity (346 $\mu\text{A}/\text{mM}/\text{cm}^2$) over the applied lower potential of +0.26 V (vs. Ag/AgCl), fast response (3 s) and broad linear range of (2–28) mM, coupled with a lower limit of detection (3.5 nM). The biosensing device gives better anti-interference ability with justifiable reproducibility, reusability (single electrode re-use 26 times in physiological buffer and 3 times in serum) and stability. Moreover, the real-time applicability of the sensor device was evaluated in human blood, serum and urine samples.

Keywords: human blood; low cost; enzyme-free; glucose; ultra-sensitive; diabetes



Citation: Imran, H.; Alam, A.; Dharuman, V.; Lim, S. Fabrication of Enzyme-Free and Rapid Electrochemical Detection of Glucose Sensor Based on ZnO Rod and Ru Doped Carbon Nitride Modified Gold Transducer. *Nanomaterials* **2022**, *12*, 1778. <https://doi.org/10.3390/nano12101778>

Academic Editors: Tai-Chia Chiu and Giuseppe Barillaro

Received: 15 April 2022

Accepted: 19 May 2022

Published: 23 May 2022

Publisher's Note: MDPI stays neutral with regard to jurisdictional claims in published maps and institutional affiliations.



Copyright: © 2022 by the authors. Licensee MDPI, Basel, Switzerland. This article is an open access article distributed under the terms and conditions of the Creative Commons Attribution (CC BY) license (<https://creativecommons.org/licenses/by/4.0/>).

1. Introduction

In 2021, worldwide, 537 million people had diabetes [1], which is one of the leading causes of death (in 2021, approximately 6.7 million deaths), compared to HIV/AIDS, tuberculosis, malaria and disability. In India, about 50.9 million people suffer from diabetes, and this ratio is likely to increase to 80 million by 2025, making it the 'Diabetes Capital' of the world. In 2021, diabetes-related health expenditure was nearly US\$966 billion [1]. Since patients with diabetes have high blood glucose, accurate determination and regular checking of blood glucose level are very important in the diagnosis and treatment of diabetes or metabolic disorders and help to reduce the death rate and economic cost. To date, different methods have been reported for the detection of glucose, such as optical [2], fluorescence [3], surface plasmon resonance [4], acoustic [5] and electrochemical methods [6–8]. Among the various detection methods, electrochemical methods have attracted much attention because of their rapid response, ease of operation, high sensitivity and excellent selectivity [6–8]. In general, two types of amperometric glucose sensors have been reported. One uses glucose oxidase (GOX) enzyme to catalyze a glucose sensor. Recently, Zhang et al. reported the GOX enzyme immobilized on CNTs-based glucose sensor [9]. The other is the direct enzyme-free electrochemical oxidation glucose sensor. Baghayeri et al. reported the Ag nanoparticles functionalized CNTs-based enzyme-free glucose sensor [10]. Between them, GOX enzyme immobilization chemistry is very difficult, and is easily affected by temperature and pH. By comparison, the enzyme-free glucose

sensor is simple, low cost and environmental free conditions. From the literature, carbon nanostructures, such as carbon nanotubes (CNTs), graphene and graphene oxides have been used to fabricate sensors based on glucose oxidase enzymes [9]. However, the highly expensive instruments and toxic chemical and safety issues in the synthesis of graphene, graphene oxide and CNTs mean that they have limited commercial applications. Very recently, most research has used as an alternative graphitic carbon nitride (g-C₃N₄). This is a 2D material and conjugated polymer that has attracted wide interdisciplinary attention as a low-cost, metal-free material with excellent electronic band structures, electron-rich properties, basic surface functions and high physicochemical stability. It has been applied in several fields, such as photosynthesis [11], H₂ evolution [12], supercapacitor [13] and sensor [7,8]. Recently, Wang et al. developed a ternary heterostructure that consists of Ru species and C–N was rationally explored for ammonia photosynthesis [14]. Chen et al. prepared graphitic C₃N₄ modified by Ru (II)-based dyes for photocatalytic H₂ evolution [15]. Shcherban et al. reported botulin oxidation over Ru nanoparticle supported on carbon nitride [16]. Peng et al. prepared Ru ion complexed carbon nitride nanosheet supported rGO as catalysts for electrochemical hydrogen evolution [17]. Recently, Hao reported a green synthesis of ruthenium modified graphitic carbon nitride nanosheet for enhanced photocatalytic ammonia synthesis [18]. However, Ru-doped g-C₃N₄ has not been attempted in the literature for glucose biosensing.

Glucose oxidase (GOX) enzyme and g-C₃N₄ modified glassy carbon electrode to detect glucose sensing with a detection limit of 11 μM was reported [19]. g-C₃N₄/αFe₂O₃ [20] and Cu²⁺-C₃N₄ [21] modified electrodes used to detect enzyme-free glucose sensor in KOH and NaOH medium were reported, with limits of detection of 0.58 and 0.35 μM, respectively. More recently, we have reported a niobium-doped carbon nitride [8] and platinum and zinc oxide modified with carbon nitride [7] for enzyme-free glucose detection in physiological buffer and obtained limits of detection of 1 and 0.1 μM, respectively. The limit of detection, linear range and selectivity limit their commercialization. To address this challenge, we have developed a simple, fast response, highly sensitive and selective enzyme-free glucose sensor at zinc oxide rod inserted ruthenium-doped carbon nitride sheet modified sensor device.

In this paper, we prepared a one-pot synthesis of ruthenium-doped graphitic carbon nitride (g-Ru-C₃N₄) sheet by an easy pyrolysis method using urea and ruthenium (III) chloride. Further, Zinc oxide rod was synthesized by precipitation method, and inserted into Ru-doped graphitic carbon nitride (ZnO-g-Ru-C₃N₄), prepared using a simple ultrasonication method. The structural and morphological properties of the sensor device were characterized by TEM, XRD, FTIR and XPS, and applied for enzyme-free glucose sensing. We tested the newly developed sensor device in human blood, serum and human urine sample, and found the developed sensor device to be highly suitable for practical and commercial application.

2. Experimental Sections

2.1. Materials and Method

Urea, ruthenium (III) chloride, zinc chloride, sodium chloride, potassium ferrocyanide, potassium ferricyanide, sodium phosphate monobasic and dibasic, D-glucose, biotin, riboflavin, fructose and galactose where all purchased from Sigma-Aldrich, St. Louis, MO, USA. Phosphate buffer solution (PBS, pH 7.4) containing 810 mL Na₂HPO₄ (100 mM) and 190 mL NaH₂PO₄ (100 mM) was used as electrolyte for all electrochemical measurements. The cyclic voltammetry (CV), electrochemical impedance spectroscopy (EIS), chronoamperometry (CA) and differential pulse voltammetry (DPV) were carried out using the SP-150 model Bio-Logic workstation (Seyssinet-Pariset, France, driven by EC-lab 11.25 software). A conventional three-electrode system was used, consisting of a gold electrode (3 mm diameter and 65 mm length) coated with synthesized materials as a working electrode, a platinum wire (0.5 mm diameter and 5 cm length) as counter and Ag/AgCl as a reference electrode. The chemical structure and morphology of the newly developed ZnO-g-Ru-C₃N₄ com-

posite materials were confirmed by X-ray diffraction (XRD, PANalytical B.V., Lelyweg 1, Almelo, The Netherlands), Energy-dispersive X-ray spectroscopy (EDS or EDX, LEO 1530 field emission from Hitachi, Japan), Fourier-transform infrared spectroscopy (FTIR, Perkin Elmer Nicolet IS10, Waltham, MA, USA), Transmission Electron Microscopy (TEM, Hitachi H-7650 electron microscopy, Tokyo, Japan) and X-ray photoelectron spectroscopy (XPS, Theta Probe AR-XPS System, Thermo Fisher Scientific UK LTD, East Grinstead, UK). The TEM and XPS instruments available at the Jeonju center KBSI, Jeonbuk National University, Republic of Korea were employed.

2.2. One-Pot Synthesis of Ruthenium-Doped Graphitic Carbon Nitride ($g\text{-Ru-C}_3\text{N}_4$)

One-pot synthesis of ruthenium-doped graphitic carbon nitride ($g\text{-Ru-C}_3\text{N}_4$) by the pyrolysis method was performed using urea and ruthenium (III) chloride (RuCl_3). Initially 20 g urea was melted, 0.1 g RuCl_3 was added, and the solution stirred well to achieve uniform dispersion. The solution was then poured into a quartz crucible and cooled to room temperature. A single crystal-like structure was formed, which was annealed at 350 °C in a tubular furnace. After the pyrolysis process, the product was washed successively with 0.1 M nitric acid, water and acetone to remove impurities and dried in air.

2.3. Sensor Device Fabrication

Five mg of the obtained ruthenium-doped graphitic carbon nitride ($g\text{-Ru-C}_3\text{N}_4$) material and 10 mg of zinc oxide rod (ZnO synthesis was followed by previous works [7]) were dispersed in 1 mL double distilled water and sonicated for 15 min. The homogeneous dispersion of $\text{ZnO-g-Ru-C}_3\text{N}_4$ was drop cast on the surface of Au electrode (2 μL) and dried in air. In addition, $g\text{-C}_3\text{N}_4$, ZnO and $g\text{-Ru-C}_3\text{N}_4$ modified Au electrodes were also prepared by the above procedure for comparison. The modified Au devices were used to study the electrochemical behavior of the surfaces and glucose oxidation.

2.4. Preparation of Analyte and Real Sample

To study the electrode sensing response, the analyte was prepared in phosphate buffer at the concentration of 100 mM for electrochemical measurement. Dynamic variation of analyte was prepared by serial dilution from 0.1 M prepared stock solution of the analytes.

Blood samples required for the experiments were collected from patients and analyses were performed in compliance with the ethical committee constituted by the Alagappa University and functioning as per ethical guidelines for biomedical research on human subjects issued by the Indian council of Medical Research (IEC/Au/2016/1/2), India. Informed consent was obtained for any experimentation with the respective patient. In this work, one blood and urine sample are used for the detection of glucose. That sample was collected from the first author. The blood and urine sample preparation and detection of glucose are followed by our previously reported processer [7,8].

3. Results and Discussion

3.1. Electrochemical Characterization of the $\text{ZnO-g-Ru-C}_3\text{N}_4$ Composite

To prove the electrochemical characteristics of the fabricated bare AuE, $g\text{-C}_3\text{N}_4$, $g\text{-Ru-C}_3\text{N}_4$, $\text{ZnO-g-Ru-C}_3\text{N}_4$ modified AuE, cyclic voltammetry (CV) performance acquired in 1 M NaOH were scanned between the potential of -0.6 V and 0.4 V at a scan rate of 50 mV s^{-1} is shown in Figure 1a. A CV signals of Ru-doped $g\text{-C}_3\text{N}_4$ shows three distinct redox peaks at -0.10 , 0.23 and 0.34 V corresponding to Ru (III/IV), Ru (IV/VI) and Ru (VI/VII) transition processes, respectively [22]. These results clearly indicate that the newly formed $g\text{-Ru-C}_3\text{N}_4$ hybrids have newer functionalities by the doping of Ru in graphitic carbon nitride structure, which are different from pure $g\text{-C}_3\text{N}_4$ and $\text{ZnO-g-Ru-C}_3\text{N}_4$ counterparts. In contrast, RuO_2 redox transition peaks on the $\text{ZnO-g-Ru-C}_3\text{N}_4$ are not well defined, they are mostly sluggish in nature and the peak current values are very minimum when compared to the $g\text{-C}_3\text{N}_4$ and $g\text{-Ru-C}_3\text{N}_4$ modified electrodes. We further examined the electrochemical characteristics of the various electrodes, CV and

EIS performance were acquired in 1 mM $[\text{Fe}(\text{CN})_6]^{3-/4-}$ as redox couple at a scan rate of 50 mV s^{-1} is shown in Figure S1. A well-resolved oxidation/reduction peak was observed in the bare AuE with an electrochemical peak separation (ΔE_p) of 88 mV and higher peak current of $7.32 \mu\text{A}$ and R_{ct} of $2043 \Omega \text{ cm}^{-2}$. A modest increase of redox peak currents ($9.58 \mu\text{A}$) with the reduced peak separation of 80 mV and R_{ct} of $1119 \Omega \text{ cm}^{-2}$ was obtained for $g\text{-C}_3\text{N}_4$ modified Au surface modified electrode. The increased electron transfer rate coupled with an enhanced current response and a reduced ΔE_p value suggest that carbon nitride contains a higher number of NH group, and it highly interacts with $[\text{Fe}(\text{CN})_6]^{3-/4-}$ ions. By modification with $g\text{-Ru-C}_3\text{N}_4$, we observed slightly decrease oxidation peak current ($8.58 \mu\text{A}$) with increased ΔE_p (90 mV) and R_{ct} of $2217 \Omega \text{ cm}^{-2}$. Similarly, the peak current response ($1.44 \mu\text{A}$) with increased peak to peak separation (110 mV) and larger R_{ct} value ($18,550 \Omega \text{ cm}^{-2}$) was observed for $\text{ZnO-g-Ru-C}_3\text{N}_4$ electrode, which might be the reason that the presence of higher amount of ZnO hampered the electron transport of $[\text{Fe}(\text{CN})_6]^{4-/3-}$ due to its semi-conductive behavior.

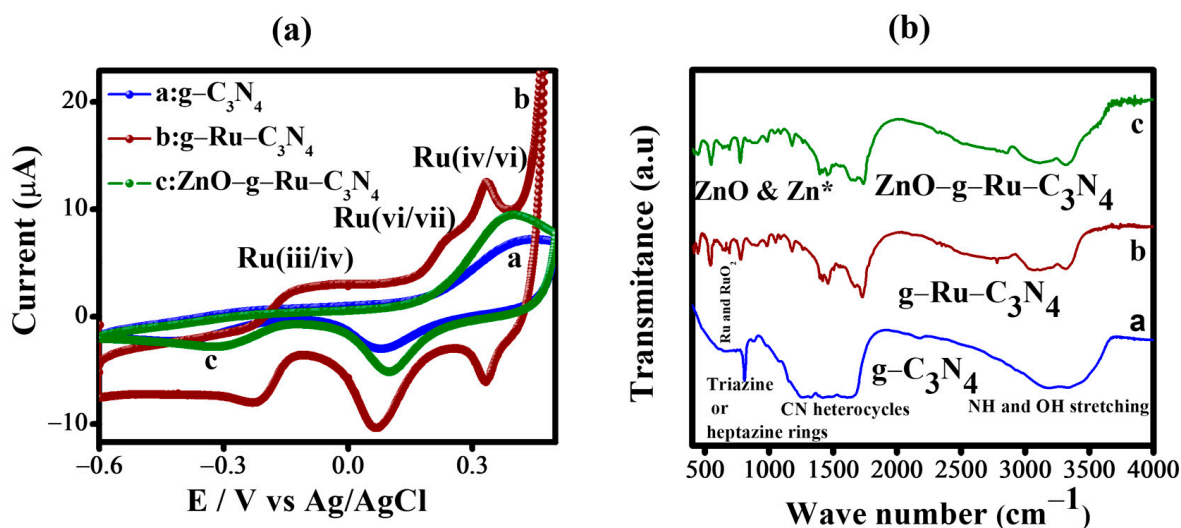


Figure 1. (a) CV behaviors of AuE- $g\text{-C}_3\text{N}_4$ (curve a), AuE- $g\text{-Ru-C}_3\text{N}_4$ (curve b) and AuE- $\text{ZnO-g-Ru-C}_3\text{N}_4$ (curve c) modified electrode in the presence of 1 M NaOH in DD water at a scan rate 50 mV s^{-1} . (b) FT-IR spectra of $g\text{-C}_3\text{N}_4$ (curve a), $g\text{-Ru-C}_3\text{N}_4$ (curve b) and $\text{ZnO-g-Ru-C}_3\text{N}_4$ (curve c). * Skeletal vibration with carbon nitride.

3.2. Physical Characterization of $\text{ZnO-g-Ru-C}_3\text{N}_4$ Composite

Figure 1b shows the FTIR spectra of $g\text{-C}_3\text{N}_4$ (curve a), $g\text{-Ru-C}_3\text{N}_4$ (curve b) and $\text{ZnO-g-Ru-C}_3\text{N}_4$ (curve c). The $g\text{-C}_3\text{N}_4$ shows a sharp absorption peak at 810 cm^{-1} for the out-of-plane bending vibration of triazine rings. The peaks at 1262 and 1421 cm^{-1} represent the aromatic CN stretching [23]. The absorption peak at 3182 cm^{-1} is attributed to $-\text{NH}$ and $-\text{OH}$ stretching. In the case of the Ru-doped $g\text{-C}_3\text{N}_4$, the triazine peak at 810 cm^{-1} is shifted and the absorption peak intensity is also decreased, compared to the $g\text{-C}_3\text{N}_4$ (810 cm^{-1}). In the spectrum, the small peaks at 662 , 540 and 444 cm^{-1} are associated with the characteristic vibrational modes of $\nu\text{Ru-O}$ and $\gamma\text{Ru-O}$, which indicate the formation of RuO_2 [24,25]. The peak at 849 cm^{-1} is attributed to the Ru-N stretching modes [26]. This result indicates Ru doped on the NH group of the carbon nitride structure. Further, zinc oxide is composited with $g\text{-Ru-C}_3\text{N}_4$. The 1459 and 555 cm^{-1} absorption peaks represent the skeletal vibration of $g\text{-C}_3\text{N}_4$ sheets and Zn-O stretching vibration, respectively [27]. These results indicate that ZnO binds with the $g\text{-Ru-C}_3\text{N}_4$ matrix. The $g\text{-C}_3\text{N}_4$ compared with the $g\text{-Ru-C}_3\text{N}_4$ and $\text{ZnO-g-Ru-C}_3\text{N}_4$, CN heterocycles, triazine and $-\text{NH}$ or $-\text{OH}$ stretching absorption peaks at 810 , 1262 , 1421 and 3182 cm^{-1} are shifted to 785 , 1406 , 1465 , 1679 , 3097 and 3322 cm^{-1} for $g\text{-Ru-C}_3\text{N}_4$, and to 778 , 1395 , 1459 , 1655 , 3093 and

3319 cm^{-1} for $\text{ZnO-g-Ru-C}_3\text{N}_4$, respectively. The FTIR results indicate the formation of the $\text{ZnO-g-Ru-C}_3\text{N}_4$ composite-like structure (Figure 1b).

The XRD patterns in Figure S2 of the Supplementary Materials show the crystalline nature and phase planes of $\text{g-C}_3\text{N}_4$, $\text{g-Ru-C}_3\text{N}_4$ and $\text{ZnO-g-Ru-C}_3\text{N}_4$. Generally, $\text{g-C}_3\text{N}_4$ contains two peaks that are found at 2θ 13.38° and 27.38°, corresponding to the 100 and 002 planes, respectively [28]. The thermally prepared $\text{g-C}_3\text{N}_4$ shows a very weak broad peak at 27.4° corresponding to the 002 plane, suggesting the absence of long-range order in the atomic arrangements in the CN. In the presence of Ru on $\text{g-C}_3\text{N}_4$, it shows increased peak intensity at 27.4°, and no new peak appears, which indicates the Ru doped on CN matrix of the structure. Further, for the ZnO decorated on $\text{g-Ru-C}_3\text{N}_4$, the 27.4° peak still appears, but the peak intensity is very low, compared to the $\text{g-C}_3\text{N}_4$ and $\text{g-Ru-C}_3\text{N}_4$. Hence, there is a high level of ZnO loading on the Ru-CN matrix. The ZnO (JCPDS: 89-7102) peaks [7] are negatively shifted, and their intensity is increased. These results indicate the formation of composite-like structure. Figure S3 of the Supplementary Materials shows the corresponding energy dispersive X-ray (EDX) spectra of $\text{g-Ru-C}_3\text{N}_4$ and $\text{ZnO-g-Ru-C}_3\text{N}_4$, revealing the presence of carbon (C), nitrogen (N) and ruthenium (Ru), with C:N:Ru ratios of 32.67:65.81:1.52. EDX analysis confirmed that the composition of the products was Ru-doped $\text{g-C}_3\text{N}_4$, without impurities. No diffraction peaks from other metals (impurities) were found, clearly showing that the structure of the carbon nitride was not affected by Ru doping, as it is doped at the outer plane of Ru-N stretching. After the ZnO nanoparticle composite with $\text{g-Ru-C}_3\text{N}_4$, Zn (75.57 %) and O (9.79 %) elements appear, and the C:N:Ru element weight percentages decrease to 5.64 : 8.07 : 0.93, compared to ruthenium doped carbon nitride (32.67:65.81:1.52), due to the high amounts of Zn and O (75.57 + 9.79 = 85.36) attach with Ru-CN matrix. These result correlate with the XRD (Figure S2), FTIR (Figure 1b) and electrochemical data (Figure 1a). Further, the morphology of the $\text{ZnO-g-Ru-C}_3\text{N}_4$ composite was studied by transmission electron microscopy (TEM). Figure 2a–c shows the TEM imagery of $\text{ZnO-g-Ru-C}_3\text{N}_4$ at different scales of 100, 20 and 5 nm. The TEM imagery clearly indicates that the carbon nitride forms a 2D sheet-like structure, and Ru nanoparticles appear in front of the sheet, and ZnO rod is inserted on the edge of the sheet. These inserted ZnO rod enhances the sensitivity and reduces the glucose oxidation potential. The chemical composition and elements of the $\text{ZnO-g-Ru-C}_3\text{N}_4$ composite are studied by XPS, as shown in Figure 2d–i. Figure 2d shows the survey spectrum of $\text{ZnO-g-Ru-C}_3\text{N}_4$ composite revealing the C, N, Ru, Zn and O elements. However, no new element peak is shown, indicating that the composite is purely composed of only C, N, Ru, Zn and O. The C 1s XPS spectrum for $\text{ZnO-g-Ru-C}_3\text{N}_4$ (Figure 2e) displays three peaks at 284.7, 288.3 and 295.3 eV. The peaks at 284.7 and 288.3 eV represented the sp^2 hybridized C–C bond [29] and the sp^2 hybridized N–C=N carbon in the aromatic tri-s-triazine rings, respectively. However, another peak at 295.3 eV is assigned to Ru 3d. The N 1s spectrum shows three peaks centered at 398.3, 399.1 and 399.9 eV, which represent the sp^2 hybridized carbon–nitrogen (C–N=C) in the aromatic triazine ring, nitrogen between the aromatic rings (–C=N) and the free amino functional groups (C–N–H) of $\text{g-C}_3\text{N}_4$, respectively [30]. The Ru 3p XPS spectrum shows one absorption peak at 461.6 eV, which represents the Ru^{4+} [31]. Figure 2h shows the XPS spectrum of Zn 2p, which reveals two peaks at 1020.3 and 1044.8 eV that correspond to the Zn 2p_{5/2} and Zn 2p_{3/2}, respectively. The Zn 2p spectrum indicates the presence of Zn ions with +2 oxidation states [32]. The O 1s XPS spectrum is deconvoluted into three peaks at 530, 531.2 and 532.3 eV, which are due to the O^{2+} , metal oxides and metal carbonate, respectively [7]. These results clearly indicate that Zn and Ru bind with the NH matrix of the structure.

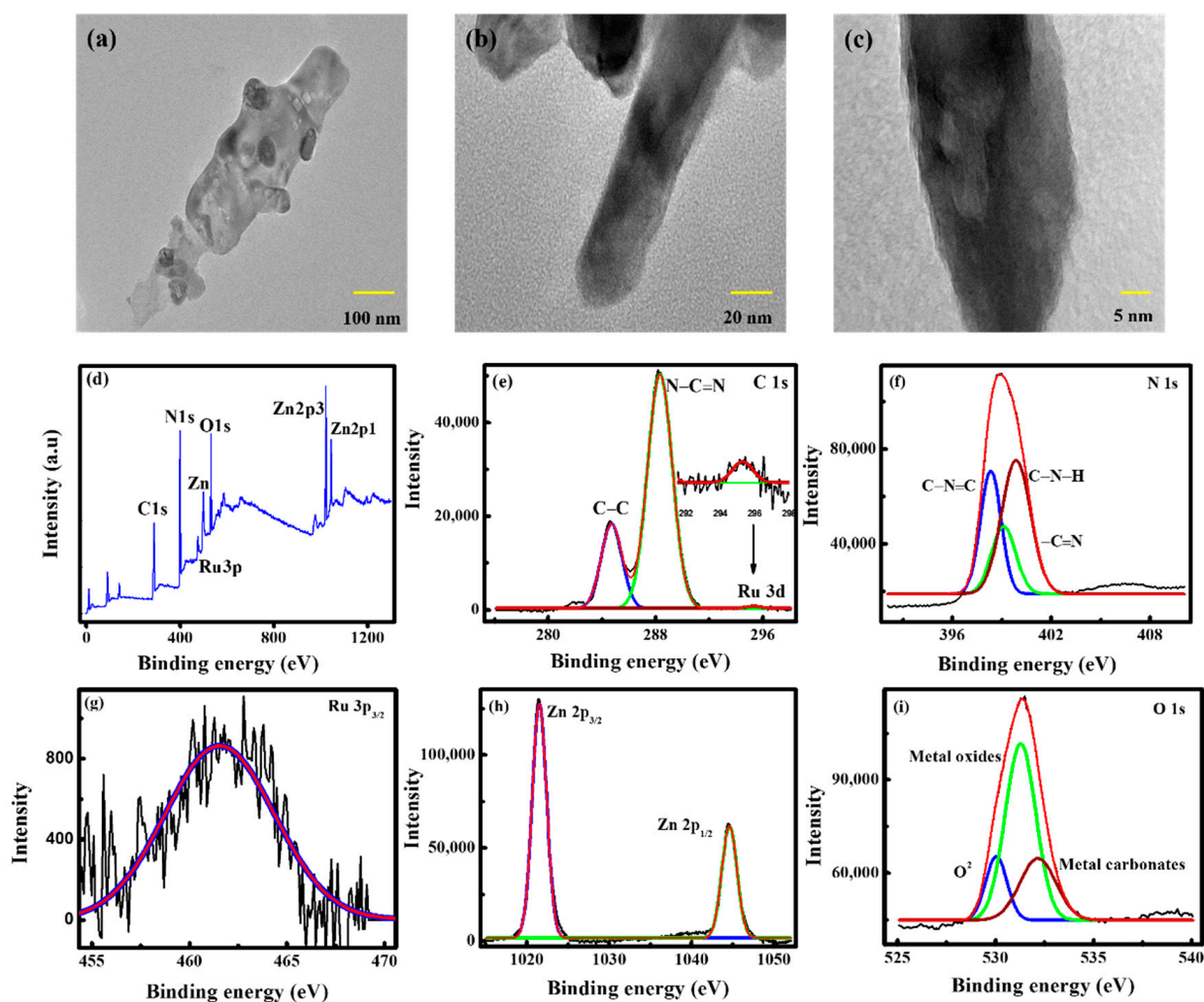
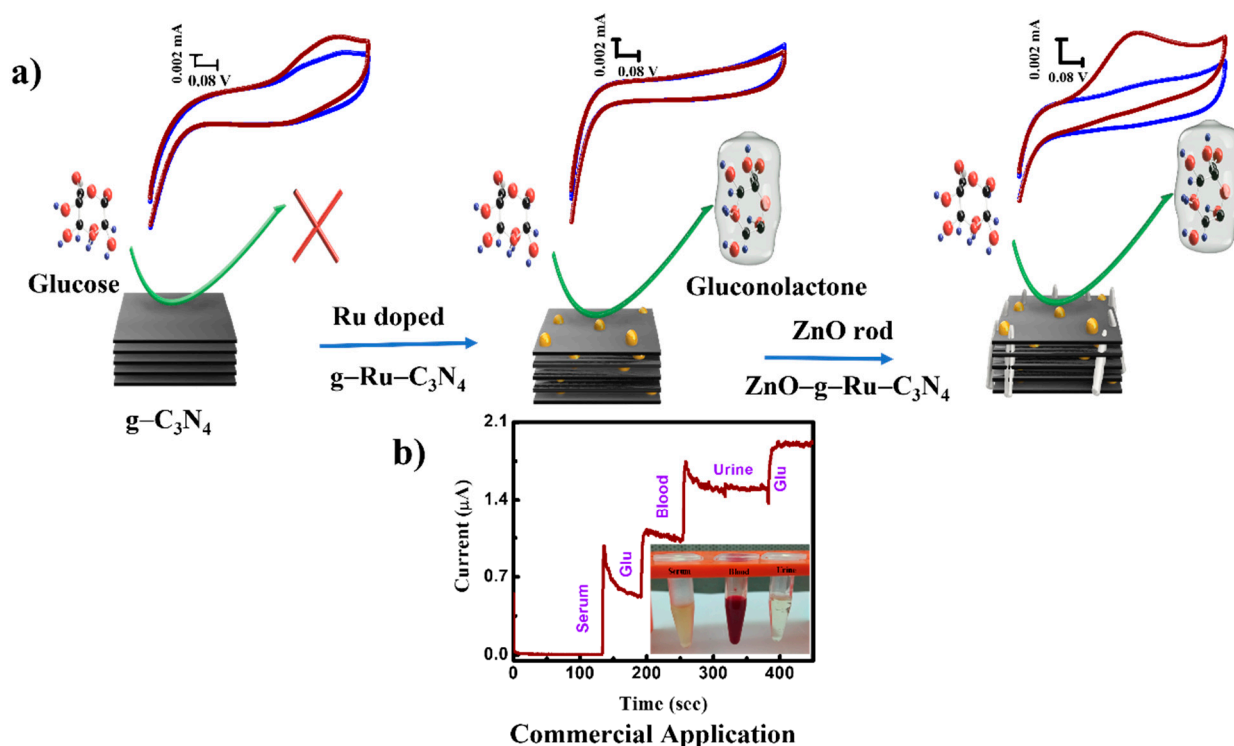


Figure 2. TEM images (a–c) and XPS spectrum (d–i) of ZnO–g–Ru–C₃N₄ composite. Surveys scan (d), C 1 s (e), N 1 s (f), Ru (g), Zn 2P (h) and O 1 s (i).

3.3. Enzyme-Free Glucose Sensing at ZnO–g–Ru–C₃N₄ Modified Sensor Device

The electrochemical characteristics of various modified electrodes were systematically performed towards the oxidation of glucose was evaluated by using CV at a scan rate of 50 mV s^{−1} in the absence and presence of 1 mM glucose in PBS. Interestingly, in the absence of glucose, all fabricated electrodes do not show any anodic peak current response. However, in the presence of glucose, the unmodified Au electrode (Figure S4a) peak current does not change in neutral pH, and this result corroborates previous report [33]. Similarly, Au electrode modified with g–C₃N₄ and ZnO was manifested only background current, which indicated an inactive electrolyte. In contrast, in the presence of glucose (1mM), a well-defined anodic peak current for glucose oxidation was obtained at 490 mV for the gold electrode modified with g–Ru–C₃N₄, implies that the g–Ru–C₃N₄ modified electrode catalyzed the glucose to gluconolactone in physiological buffer (Scheme 1, Figure 3) without aid of enzyme. Upon the modification of the gold electrode with ZnO rod decorated on Ru-doped carbon nitride (ZnO–g–Ru–C₃N₄), the oxidation peak current enhances remarkably (6.9×10^{-7} A), which is much higher than the g–Ru–C₃N₄ modified electrode (Figure 1). In addition, oxidation peak potential is negatively shifted (260 mV), compared to g–Ru–C₃N₄ (E_{pa} 490 mV) modified electrode. The outstanding electrochemical properties of the electrode are believed to be due to the synergistic interaction between g–Ru–C₃N₄ and ZnO nanorod, which accentuated the electrode's electro-catalytic properties. Metal and/or metal oxide modified surface catalyzing the glucose oxidation is reported by Hsia

et al. [34]. Hydroxyl ions are adsorbed on the ZnO-g-Ru-C₃N₄ modified surface, and act as a glucose oxidation mediator and surface oxygen reduction reaction. ZnO-g-Ru-C₃N₄ modified electrode catalyzes the glucose to gluconolactone, releasing two protons per glucose molecule (Scheme 1). Furthermore, the optimization of the ratio between the g-Ru-C₃N₄ and ZnO was studied by preparing the ZnO-g-Ru-C₃N₄ composites at different ratio (1:1, 1:2 and 2:1), and measured in PBS (pH 7.4) in the absence (curve a) and presence (curve b) of 1 mM glucose at a scan rate of 50 mV s⁻¹ (Figure S5). Note that the ZnO-g-Ru-C₃N₄ composite prepared at 1:2 ratio exhibits the highest glucose oxidation compared to the other ratios (1:1 and 2:1). Thus, 1:2 ratio of g-Ru-C₃N₄ and ZnO is used for further electrochemical and physical characterization, and to optimize the glucose sensing properties.



Scheme 1. (a) Enzyme-free glucose sensing at ZnO rod inserted Ru doped carbon nitride modified sensor devices. (b) Developed sensor device practically tested in human blood, blood serum and urine samples.

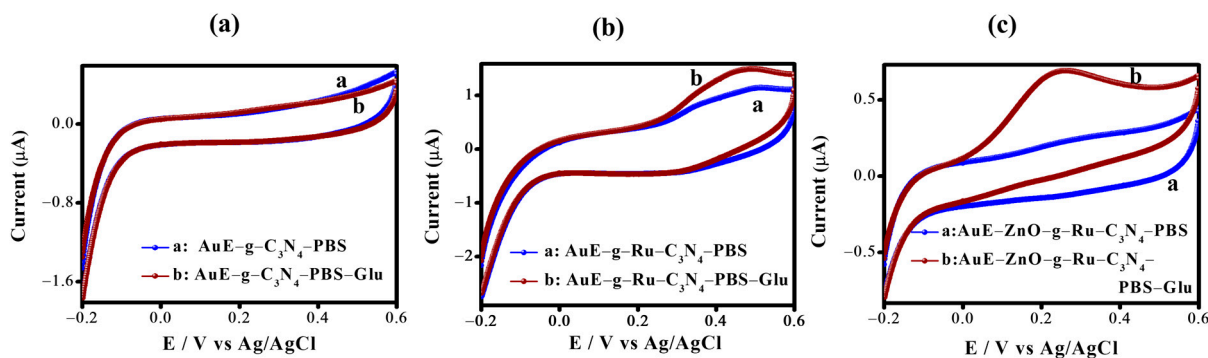


Figure 3. CV behavior of g-C₃N₄ (a), g-Ru-C₃N₄ (b) and ZnO-g-Ru-C₃N₄ (c) modified electrode and used for the glucose sensing. Measured in PBS in the absence (curve a) and presence (curve b) of 1 mM glucose at a scan rate 50 mV s⁻¹.

3.4. Effect of the Scan Rate and pH on the ZnO-g-Ru-C₃N₄ Modified Sensor Device

Figure S6 of the Supplementary Materials shows the effect of the scan rate varied from 10 to 100 mV s⁻¹ in the presence of 1 mM glucose in PBS. From the result, the scan rate is increased and the glucose oxidation peak current also increases, due to its diffusion-controlled (1.75×10^{-6} cm⁻¹) oxidation of glucose to gluconolactone [35–40]. Next, the effect of the pH on the ZnO-g-Ru-C₃N₄ modified electrode in the presences of 1 mM glucose oxidation peak current and peak potential was carefully monitored by CV using 100 mM PBS in different pH ranging (5, 5.5, 6, 7, 7.4, 8 and 8.5) at a scan rate 50 mV s⁻¹ in Figure 4. It is apparent that the glucose oxidation peak current is increased to pH 7.4, then the oxidation peak current is decreased. From Figure 4, the highest glucose oxidation peak current is obtained at pH 7.4. In addition, as the PBS solution pH (5 to 8.5) was gradually increased, the glucose oxidation peak potential was positively shifted, which indicates that protons are involved in the electrode processes [41,42]. These results indicate that pH of 7.4 results in higher glucose oxidation current, and it was used for further optimization studies. The Nernst equation ($\Delta E_p / (58.65 \Delta \text{pH}) = n$) is used to calculate the number of electrons involved in the oxidation reaction. From slope of pH versus peak potential (E_p), obtained 51 mV/pH for the oxidation of glucose, which indicates one electron transfer during the rate-determining step.

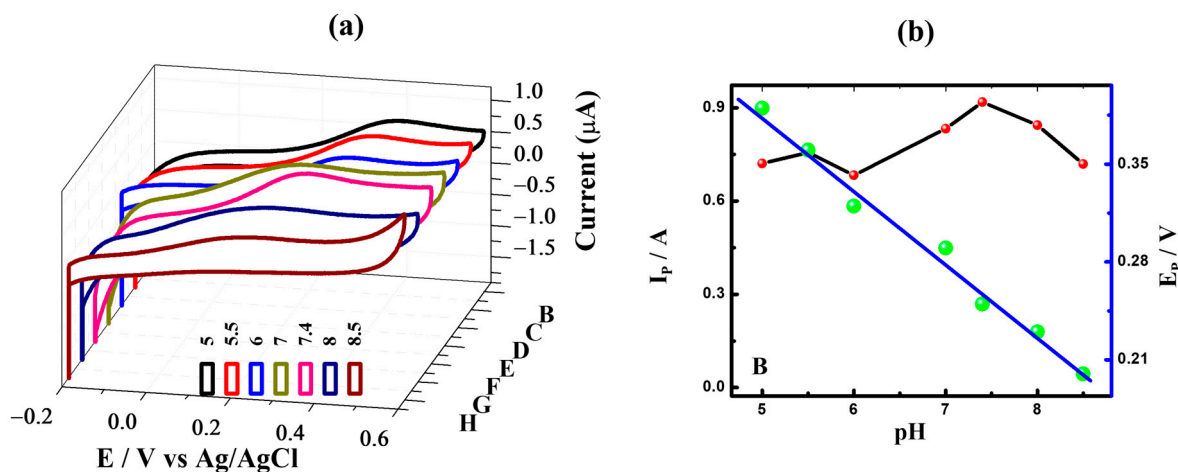


Figure 4. (a) CV behaviour of ZnO-g-Ru-C₃N₄ electrode in the presences of 1 mM glucose in different pHs (5 (B), 5.5 (C), 6, (D), 7 (E), 7.4 (F), 8 (G) and 8.5 (H)) solution. (b) pH versus peak current (left) and peak potential (right) measured from the corresponding CV behavior.

3.5. Effect of Glucose Concentration on the ZnO-g-Ru-C₃N₄ Modified Sensor Device

Figure 5a demonstrates the amperometry behavior of the newly developed ZnO-g-Ru-C₃N₄ modified surface with 2 mM glucose concentration sequentially added at every 50 s up to 28 mM at an applied potential of +0.26 V under the stirring condition in 100 mM PBS solution. By the successive addition of different concentration of glucose, within 3 s, the electrocatalytic oxidation current quickly increases, and the maximum signal/noise ratio 0.9 is observed. The insert images show the linear increase of glucose concentration with an increase of current and the r^2 (0.99) values are found to be high. Figure 5b plots the log glucose concentration versus log current. From the figure, the higher glucose concentration linear ranges 2 to 28 mM with r^2 value of 1. These newly developed ZnO-g-Ru-C₃N₄ modified sensor device are suitable for applying Michaelis–Menten (MM) kinetics. From the line weaver Burk plot (Figure 5c), a linear equation is obtained of $I^{-1} = (8.16 \times 10^3) \times [\text{glucose}]^{-1} + (1.24 \times 10^3)$. The K_M is calculated as 65 mM, which is the highest K_M value, compared to the g-C₃N₄ based systems.

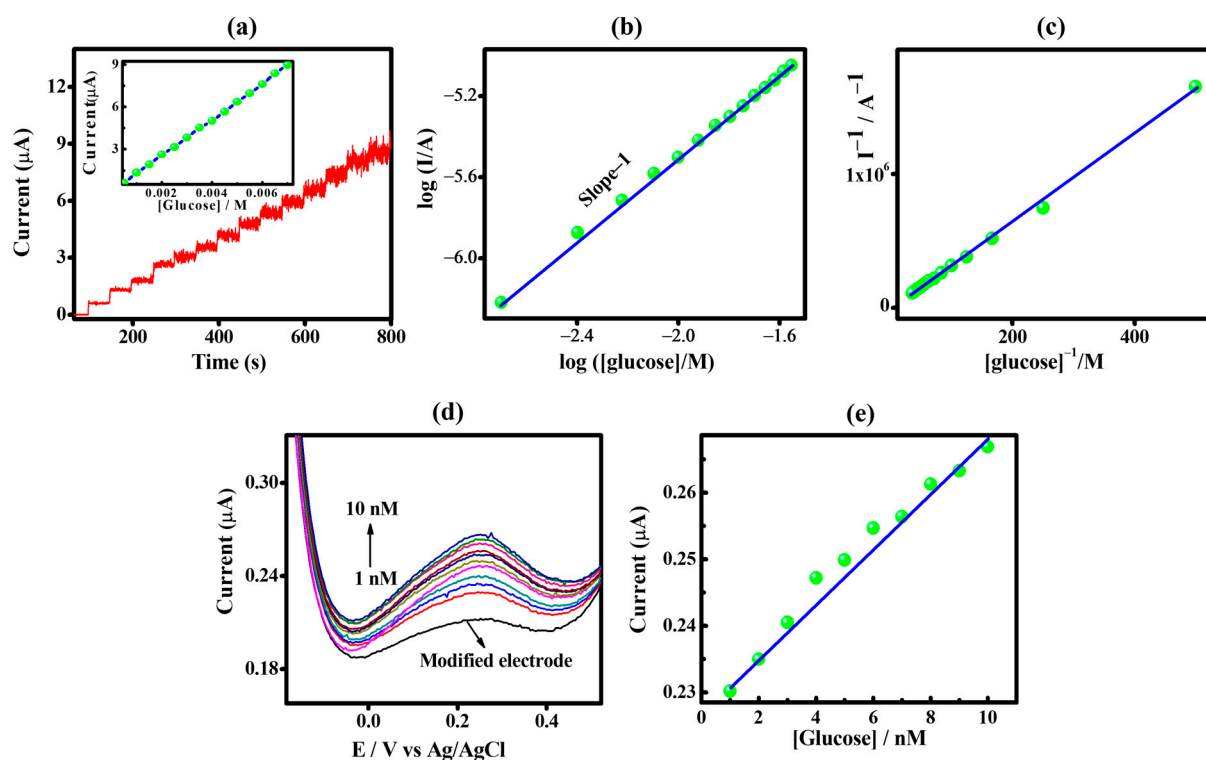


Figure 5. (a) Effect of different glucose concentration on CA behavior of ZnO-g-Ru-C₃N₄ measured at 0.26 V in PBS pH 7.4. Concentration range 2 to 26 mM and inset glucose concentration versus current plot. (b) log concentration versus log current. (c) Line weaver Burk plot (1/current vs. 1/[glucose]). (d) Effect of glucose concentration on DPV behavior of ZnO-g-Ru-C₃N₄ measured in PBS pH 7.4. Concentration range 1 to 10 nM (d) for ZnO-g-Ru-C₃N₄ modified electrode and (e) glucose concentration versus current plot.

Further, the limit of detection (LOD) is calculated from the difference pulse voltammetry (DPV) in Figure 5d,e. The ZnO-g-Ru-C₃N₄ shows good linearity, even in a low concentration range of 1 to 10 nM and a correlation coefficient of 0.99. The LOD has been theoretically calculated using the formula $3 \times$ standard deviation of the blank signal (4.71×10^{-9} A)/slope of the calibration curve (4.029 A/M) which gives the LOD 3.5 nM. The detection performance of the fabricated modified electrode is compared with other reported g-C₃N₄ based non-enzymatic glucose sensors. As shown in Table 1 [7,8,19–21] it is worth mentioning that the ZnO-g-Ru-C₃N₄ modified electrode exhibits outstanding electrocatalytic performance for glucose sensing in terms of ultra-high sensitivity, lower detection limit and wide linear range.

Table 1. Carbon nitride-based glucose sensing system.

Surface	Method	Electrolyte	Limit of Detection (LOD)	Reference
ZnO-g-Pt-C ₃ N ₄	Electrochemical method	PBS	0.1 µM	[7]
g-Nb-C ₃ N ₄	Electrochemical method	PBS	1 µM	[8]
g-C ₃ N ₄ -GOx/GCE	Electrochemical method	PBS	11 µM	[19]
g-C ₃ N ₄ /α-Fe ₂ O ₃	Electrochemical method	KOH	0.58 µM	[20]
Cu ²⁺ -C ₃ N ₄ /MWCNT	Electrochemical method	NaOH	0.35 µM	[21]
ZnO-g-Ru-C ₃ N ₄	Electrochemical method	PBS	3.5 nM	This work

3.6. Selectivity, Stability and Reproducibility of the ZnO-g-Ru-C₃N₄ Modified Sensor Device

Selectivity, stability and reproducibility are important parameters for developing a new sensor device. The selectivity of the ZnO-g-Ru-C₃N₄ modified electrode for glucose

sensing was studied by chronoamperometric (CA) detection using the same potential interferences as 0.1 mM fructose, galactose, NaCl, KCl, H₂O₂, uric acid, epinephrine, serotonin, biotin, bilirubin and riboflavin in 100 mM PBS that are present in Figure S7 of the Supplementary Materials. The potential interferences were added, respectively, in the same solution. These results clearly indicate that only the strong glucose oxidation peak current was observed, and very small current response was observed for other potential interferences. From Figure S7, the sensitivity of the developed sensor was 346 $\mu\text{A mM}^{-1} \text{cm}^{-2}$ and in the presence of potential interference (such as uric acid) sensitivity of the sensor slightly increase to 354 $\mu\text{A mM}^{-1} \text{cm}^{-2}$.

Figure S8 of the Supplementary Materials shows the 20 days (d) continuous monitoring of the ZnO-g-Ru-C₃N₄ modified electrode in the presence of 1 mM glucose in PBS at a scan rate 50 mV s⁻¹ using the CV method. The anodic glucose oxidation peak current is plotted against the number of days. Compared to the day 1 oxidation peak current, only 0.6% loss was shown for day 20. These results indicate that the ZnO-g-Ru-C₃N₄ modified electrode shows high stability up to day 20. Further surface reproducibility is tested using 4 different ZnO-g-Ru-C₃N₄ modified electrodes in the presence of 1 mM glucose (Figure S9 of the Supplementary Materials). The 4 modified different electrodes show similar oxidation potential and peak current, which indicates that the surface is highly reproducible.

3.7. Reusability of the ZnO-g-Ru-C₃N₄ Modified Sensor Device

An enzyme-free and reusable surface is needed for low-cost glucose strip fabrication. In this regard, we have tested the reusability of electrode surface in PBS and blood serum. Figure S10 of the Supplementary Materials plots the anodic glucose oxidation current versus the number of times reusable in a single electrode. From the figure, the ZnO-g-Ru-C₃N₄ modified single sensor device is reusable in PBS for 26 times and in serum for 3 times. These results indicate that the ZnO-g-Ru-C₃N₄ modified electrode shows high sensitivity, very low limit of detection, selectivity, reproducibility, stability and reusability. In this regard, the newly developed sensor device was further tested for practical application.

3.8. Practical Application

The treatment of diabetic-related diseases is purely dependent upon the monitoring of glucose in human blood, blood serum and urine samples (Figure S11 of the Supplementary Materials). Hence, the commercial applicability of the newly developed ZnO-g-Ru-C₃N₄ modified sensor device was further tested for the detection of glucose in human blood, blood serum and urine samples by the chronoamperometric method. Blood and urine samples were collected from first author. The blood, serum and urine samples were successfully added in 100 mM PBS, and their corresponding amperometric response was noticed. In blood and serum, a good response was observed, while in the urine sample, no response was observed. This result indicates that the ZnO-g-Ru-C₃N₄ modified electrode selectively detects glucose only. The advantages of the newly fabricated electrode for glucose sensor are its simplicity, high sensitivity, very low limit of detection, selectivity and reusability.

4. Conclusions

A novel zinc oxide rod inserted Ru-doped graphitic carbon nitrate was prepared by a simple mixing method (5 mg g-Ru-C₃N₄ and 10 mg ZnO). In NaOH, the Ru-doped g-C₃N₄ showed three redox peaks of Ru(iii/iv), Ru(vi/vii) and Ru(iv/vi), which confirmed that the Ru nanoparticles were attached onto the CN matrix. After ZnO was composited on g-Ru-C₃N₄, these three redox peaks disappeared, which indicates the formation of composite-like structure. The chemical investigation using FTIR found 444, 540, 662, 849, 1459 and 555 cm⁻¹ peaks that confirmed the Ru and ZnO on the g-C₃N₄ matrix. This binding may be due to the strong interaction of ZnO and Ru particles, and the N-H stretching group in the carbon nitride. The morphology of the composite was studied using TEM. Finally, the transducer was tested for enzyme-free glucose sensing by cyclic

voltammetry, chronoamperometry and differential pulse voltammetry measurement, which results indicate the better linearity of 2 to 28 mM, high sensitivity ($346 \mu\text{A}/\text{mM}/\text{cm}^2$), selectivity, very low limit of detection (3.5 nM), stability and reusability. This modified single sensor device is re-used 26 times in PBS and 3 times in blood serum. The practicability of the sensor is proved through the real-time determination of the glucose level in human blood, blood serum and urine samples. The overall results show that the ZnO-g-Ru-C₃N₄ modified electrode is a suitable platform for the clinical analysis of glucose.

Supplementary Materials: The following supporting information can be downloaded at: <https://www.mdpi.com/article/10.3390/nano12101778/s1>, Figure S1: CV (A) EIS (B) behaviors of AuE (curve a), AuE-g-C₃N₄ (curve b), AuE-ZnO (Curve c), AuE-g-Ru-C₃N₄ (curve d) and AuE-ZnO-g-Ru-C₃N₄. Measurements are made in presence of [Fe(CN)₆]^{3-/4-} in PBS (pH 7.4). Star line: [R(Q(RW))] circuit fit data.; Figure S2: XRD pattern (A) of g-C₃N₄ (curve a), g-Ru-C₃N₄ (curve b), and ZnO-g-Ru-C₃N₄ (B); Figure S3: Energy dispersive X-ray (EDX) analyses of Ru-doped g-C₃N₄ (A) and ZnO-g-Ru-C₃N₄ (B); Figure S4: CV behavior of unmodified gold electrode (A) and ZnO (B) modified electrode in the absences (curve a) and presences (curve b) of 1 mM glucose in PBS at a scan rate of 50 mV s⁻¹; Figure S5: Effect of different ratio of g-Ru-C₃N₄ and ZnO mixture (ratio 1:1 (A), 1:2 (B) and 2:1 (C)) used for AuE modification and used for the glucose sensing. Measured in PBS in the absences (curve a) and presences (curve b) of 1 mM glucose at a scan rate 50 mV s⁻¹; Figure S6: (A) Effect of varying scan rate on the CV behavior of ZnO-g-Ru-C₃N₄. (B) Corresponding plots of (scan rate)^{1/2} versus current.; Figure S7: Selective sensing of glucose with the potential interferences are fructose, galactose, riboflavin, bilirubin, biotin, NaCl, KCl, H₂O₂, uric acid, serotonin and epinephrine with the concentration of 0.1 mM in PBS.; Figure S8: Study of stability of ZnO-g-Ru-C₃N₄ modified electrode monitored voltammetrically in presence of 1mM glucose in PBS. Anodic peak current is plotted against Number of days.; Figure S9: Reproducibility data obtained on using four different gold electrodes of similar activity for modifying with ZnO-g-Ru-C₃N₄. Measured in PBS in the absences (curve a) and presences (curve b) of 1 mM glucose at a scan rate of 50 mV s⁻¹; Figure S10: Reusable single electrode is measured in PBS (A) in the presences of 1 mM glucose at a scan rate of 50 mV s⁻¹. (B) Blood serum.; Figure S11: Developed sensor device practically tested in human blood, blood serum and urine samples.

Author Contributions: H.I.: Conceptualization, literature search, data curation, formal analysis, methodology, writing—original draft. A.A.; literature search, data curation, formal analysis, methodology. V.D.; investigation, supervision, validation, writing—review and editing. S.L.; investigation, supervision, validation, funding acquisition, writing—review and editing. All authors have read and agreed to the published version of the manuscript.

Funding: This work was supported by a National Research Foundation of Korea (NRF) grant, funded by the Korea government (2021R1A2C1011248).

Institutional Review Board Statement: Blood samples required for the experiments were collected from patients and analyses were performed in compliance with the ethical committee constituted by the Alagappa University and functioning as per ethical guidelines for biomedical research on human subjects issued by the Indian council of Medical Research (IEC/Au/2016/1/2), India. Informed consent was obtained for any experimentation with the respective patient.

Informed Consent Statement: In this work, one blood, serum and urine sample are used for the detection of glucose. That sample was collected from the first author.

Data Availability Statement: Not applicable.

Conflicts of Interest: The authors declare that they have no known competing financial interests or personal relationships that could have appeared to influence the work reported in this paper.

References

1. IDF DIABETES ATLAS 10th Edition 2021 (PDF). Available online: www.diabetesatlas.org (accessed on 7 July 2021).
2. Steiner, M.S.; Duerkop, A.; Wolfbeis, O.S. Optical methods for sensing glucose. *Chem. Soc. Rev.* **2011**, *40*, 4805–4839. [[CrossRef](#)] [[PubMed](#)]
3. Tian, J.; Liu, S.; Luo, Y.; Sun, X. Fe (III)-based coordination polymer nanoparticles: Peroxidase-like catalytic activity and their application to hydrogen peroxide and glucose detection. *Catal. Sci. Technol.* **2012**, *2*, 432–436. [[CrossRef](#)]

4. Close, N.J.; Ronkainen, H.B.; Halsall, W.R. Heineman Electrochemical biosensors. *Chem. Soc. Rev.* **2010**, *39*, 1747–1763.
5. Luo, J.; Luo, P.; Xie, M.; Du, K.; Zhao, B.; Pan, F.; Fan, P.; Zeng, F.; Zhang, Z.; Liang, G. A new type of glucose biosensor based on surface acoustic wave resonator using Mn-doped ZnO multilayer structure. *Biosens. Bioelectron.* **2013**, *49*, 512–518. [[CrossRef](#)]
6. Adeel, M.; Asif, K.; Rahman, M.; Daniele, S.; Canzonieri, V.; Rizzolio, F. Glucose Detection Devices and Methods Based on Metal–Organic Frameworks and Related Materials. *Adv. Funct. Mater.* **2021**, *31*, 2106023. [[CrossRef](#)]
7. Imran, H.; Vaishali, K.; Francy, S.A.; Manikandan, P.N.; Dharuman, V. Platinum and zinc oxide modified carbon nitride electrode as non-enzymatic highly selective and reusable electrochemical diabetic sensor in human blood. *Bioelectrochemistry.* **2021**, *137*, 107645. [[CrossRef](#)]
8. Imran, H.; Manikandan, P.N.; Dharuman, V. Highly selective and rapid non-enzymatic glucose sensing at ultrathin layered Nb doped C₃N₄ for extended linearity range. *Microchem. J.* **2021**, *160*, 105774. [[CrossRef](#)]
9. Adeel, M.; Rahman, M.; Caligiuri, I.; Canzonieri, V.; Rizzolio, F.; Daniele, S. Recent advances of electrochemical and optical enzyme-free glucose sensors operating at physiological conditions. *Biosens. Bioelectron.* **2020**, *165*, 112331. [[CrossRef](#)]
10. Juska, V.B.; Pemble, M.E. A Critical Review of Electrochemical Glucose Sensing: Evolution of Biosensor Platforms Based on Advanced Nanosystems. *Sensors* **2020**, *20*, 6013. [[CrossRef](#)]
11. Wang, L.; Wang, K.; He, T.; Zhao, Y.; Song, H.; Wang, H. Graphitic Carbon Nitride-Based Photocatalytic Materials: Preparation Strategy and Application. *Chem. Eng.* **2020**, *8*, 16048–16085. [[CrossRef](#)]
12. Shinde, S.S.; Samia, A.; Lee, J.-H. Electrocatalytic hydrogen evolution using graphitic carbon nitride coupled with nanoporous graphene co-doped by S and Se. *J. Mater. Chem. A* **2015**, *3*, 12810–12819. [[CrossRef](#)]
13. Lin, Z.; Wang, K.; Wang, X.; Wang, S.; Pan, H.; Liu, Y.; Xu, S.; Cao, S. Carbon-Coated Graphitic Carbon Nitride Nanotubes for Supercapacitor Applications. *ACS Appl. Nano Mater.* **2020**, *3*, 7016–7028. [[CrossRef](#)]
14. Wang, H.; Li, X.; Ruan, Q.; Tang, J. Ru and RuO_x decorated carbon nitride for efficient ammonia photosynthesis. *Nanoscale* **2020**, *12*, 12329–12335. [[CrossRef](#)] [[PubMed](#)]
15. Chen, Y.; Liu, Y.; Ma, Z. Graphitic C₃N₄ modified by Ru (II)-based dyes for photocatalytic H₂ evolution. *Colloids Surf. A Physicochem. Eng. Asp.* **2021**, *614*, 126119. [[CrossRef](#)]
16. Shcherban, N.D.; Mäki-Arvela, P.; Aho, A.; Sergiienko, S.A.; Skoryk, M.A.; Kolobova, E.; Simakova, I.L.; Eränen, K.; Smeds, A.; Hemming, J.; et al. Preparation of betulone via betulic acid oxidation over Ru nanoparticles deposited on graphitic carbon nitride. *Catal. Lett.* **2019**, *149*, 723–732. [[CrossRef](#)]
17. Peng, Y.; Pan, W.; Wang, N.; Lu, J.-E.; Chen, S. Ruthenium ion-complexed graphitic carbon nitride nanosheets supported on reduced graphene oxide as high-performance catalysts for electrochemical hydrogen evolution. *ChemSusChem* **2018**, *11*, 130–136. [[CrossRef](#)]
18. Hao, D.; Ren, J.; Wang, Y.; Arandiyan, H.; Garbrecht, M.; Bai, X.; Shon, H.K.; Wei, W.; Ni, B.-J. A green synthesis of Ru modified g-C₃N₄ nanosheets for enhanced photocatalytic ammonia synthesis. *Energy Mater. Adv.* **2021**, *12*, 9761263. [[CrossRef](#)]
19. Tian, J.; Liu, Q.; Ge, C.; Xing, Z.; Asiri, A.M.; Al-Youbi, A.O.; Sun, X. Ultrathin graphitic carbon nitride nanosheets: A low-cost, green, and highly efficient electrocatalyst toward the reduction of hydrogen peroxide and its glucose biosensing application. *Nanoscale* **2012**, *5*, 8921–8924. [[CrossRef](#)]
20. Liu, L.; Wang, J.; Wang, C.; Wang, G. Facile synthesis of graphitic carbon nitride/nanostructured α -Fe₂O₃ composites and their excellent electrochemical performance for supercapacitor and enzyme-free glucose detection applications. *Appl. Surf. Sci.* **2016**, *390*, 303–310. [[CrossRef](#)]
21. Zheng, W.; Li, Y.; Liu, M.; Tsang, C.-S.; Yoon, L.; Lee, S.; Wong, K.-Y. Cu²⁺ doped carbon nitride/MWCNT as an electrochemical glucose sensor. *Electroanalysis* **2018**, *30*, 1446–1454. [[CrossRef](#)]
22. Doyle, R.L.; Godwin, I.J.; Brandon, M.P.; Lyons, M.E.G. Redox and electrochemical water splitting catalytic properties of hydrated metal oxide modified electrodes. *Phys. Chem. Chem. Phys.* **2013**, *15*, 13737–13783. [[CrossRef](#)] [[PubMed](#)]
23. Bojdys, M.J.; Muller, J.-O.; Antonietti, M.; Thomas, A. Ionothermal synthesis of crystalline condensed graphitic carbon nitride. *Chem.–Eur. J.* **2008**, *14*, 8177–8182. [[CrossRef](#)] [[PubMed](#)]
24. Mink, J.; Kristof, J.; Battisti, A.D.; Daalio, S.; Nemeth, C. Investigation on the formation of RuO₂ based mixed oxide coatings by spectroscopic methods. *Surf. Sci.* **1995**, *335*, 252–257. [[CrossRef](#)]
25. Borah, G.; Sharma, P. A novel route to size and shape controlled synthesis of DMSO capped ruthenium dioxide nanoparticles. *Indian J. Chem.* **2011**, *50*, 41–45.
26. Jin, C.; Bigdeli, F.; Jin, Z.-M.; Xie, Y.-R.; Hu, M.-L.; Morsali, A. Ultrasonic effect on RuO₂ nanostructures prepared by direct calcination of two new Ru(II)-organic supramolecular polymers. *Ultrason. Sonochem.* **2017**, *39*, 420–429. [[CrossRef](#)]
27. Saranya, M.; Ramachandran, R.; Wang, F. Graphene-zinc oxide (G-ZnO) nanocomposite for electrochemical supercapacitor applications. *J. Sci. Adv. Mater. Devices* **2016**, *1*, 454–460. [[CrossRef](#)]
28. Zhang, G.; Zhang, J.; Zhang, M.; Wang, X. Polycondensation of thiourea into carbon nitride semiconductors as visible light photocatalysts. *J. Mater. Chem.* **2012**, *22*, 8083–8091. [[CrossRef](#)]
29. Imran, H.; Manikandan, P.N.; Dharuman, V. Ultra-sensitive and selective label free electrochemical DNA detection at layer-by-layer self-assembled graphene oxide and vesicle liposome nano-architecture. *J. Electroanal. Chem.* **2019**, *835*, 10–21. [[CrossRef](#)]
30. Gu, S.; Xie, J.; Li, C.M. Hierarchically porous graphitic carbon nitride large-scale facile synthesis and its application toward photocatalytic dye degradation. *RSC Adv.* **2014**, *4*, 59436. [[CrossRef](#)]

31. Wang, P.; Liu, H.; Tan, Q.; Yang, J. Ruthenium oxide-based nanocomposites with high specific surface area and improved capacitance as a supercapacitor. *RSC Adv.* **2014**, *4*, 42839. [[CrossRef](#)]
32. Kalisamy, P.; Lallimathi, M.; Suryamathi, M.; Palanivel, B.; Venkatachalam, M. ZnO- embedded S-doped g-C₃N₄ heterojunction: Mediator-free Z-scheme mechanism for enhanced charge separation and photocatalytic degradation. *RSC Adv.* **2020**, *10*, 28365. [[CrossRef](#)] [[PubMed](#)]
33. Pasta, M.; La Mantia, F.; Cui, Y. Mechanism of glucose electrochemical oxidation on gold surface. *Electrochim. Acta* **2010**, *55*, 5561–5568. [[CrossRef](#)]
34. Hsiao, M.W.; Adzic, R.R.; Yeager, E.B. Electrochemical oxidation of glucose on single crystal and polycrystalline gold surfaces in phosphate buffer. *J. Electrochem. Soc.* **1996**, *143*, 759–767. [[CrossRef](#)]
35. Bhat, K.S.; Byun, S.; Alam, A.; Ko, M.; An, J.; Lim, S. A fast and label-free detection of hydroxymethylated DNA using a nozzle-jet printed AuNPs@Ti₃C₂ MXene-based electrochemical sensor. *Talanta* **2022**, *244*, 123421. [[CrossRef](#)]
36. Saeed, G.; Alam, A.; Bandyopadhyay, P.; Jeong, S.M.; Kim, K.H.; Lim, S. Metal-organic framework-derived (Mn-1)Co_xS_y@(Ni-Cu)OHs marigold flower-like core@shell as cathode and (Mn-Fe₁₀)S_x@graphene-foam as anode materials for ultra-high energy-density asymmetric supercapacitor. *Mater. Today Chem.* **2022**, *23*, 100758. [[CrossRef](#)]
37. Alam, A.; Saeed, G.; Lim, S. One-step synthesis of 2D-2D Co(OH)₂-MoSe₂ hybrid nanosheets as an efficient electrode material for high-performance asymmetric supercapacitor. *J. Electroanal. Chem.* **2020**, *879*, 114775. [[CrossRef](#)]
38. Alam, A.; Saeed, G.; Hong, S.M.; Lim, S. Development of 3D-Printed MWCNTs/AC/BNNTs Ternary Composite Electrode Material with High-Capacitance Performance. *Appl. Sci.* **2021**, *11*, 2636. [[CrossRef](#)]
39. Bhat, K.S.; Kim, H.; Alam, A.; Ko, M.; An, J.; Lim, S. Rapid and Label-Free Detection of 5Hydroxymethylcytosine in Genomic DNA Using an Au/ZnO Nanorods Hybrid Nanostructure-Based Electrochemical Sensor. *Adv. Healthc. Mater.* **2021**, *10*, 2101193. [[CrossRef](#)]
40. Alam, A.; Saeed, G.; Kim, K.H.; Lim, S. Sonochemical synthesis of welded titanium dioxide-silver nanocomposite as a 3-dimensional direct ink writing printed cathode electrode material for high-performance supercapacitor. *J. Energy Storage* **2022**, *45*, 103524. [[CrossRef](#)]
41. Pereira, S.O.; Santos, N.F.; Carvalho, A.F.; Fernandes, A.J.S.; Costa, F.M. Electrochemical Response of Glucose Oxidase Adsorbed on Laser-Induced Graphene. *Nanomaterials* **2021**, *11*, 1893. [[CrossRef](#)]
42. Ksenzhek, O.S.; Petrova, S.A. Electrochemical properties of flavins in aqueous solutions. *J. Electroanal. Chem. Interfacial Electrochem.* **1983**, *11*, 105–127. [[CrossRef](#)]